Distributed Traffic Control for Reduced Fuel Consumption and Travel Time in Transportation Networks

**Final Report
April 2018**

MIDWEST
TRANSPORTATION
CENTER **MTC**

IOWA STATE UNIVERSITY
Institute for Transportation

Technical Report Documentation Page

1. Report No.	2. Government Accession No.	3. Recipient's Catalog No.

4. Title and Subtitle	5. Report Date
Distributed Traffic Control for Reduced Fuel Consumption and Travel Time in Transportation Networks	April 2018
	6. Performing Organization Code

7. Author(s)	8. Performing Organization Report No.
Yue Zu, Chenhui Liu, Ran Dai, Anuj Sharma, and Jing Dong	

9. Performing Organization Name and Address	10. Work Unit No. (TRAIS)
Institute for Transportation Iowa State University 2711 South Loop Drive, Suite 4700 Ames, IA 50010-8664	
	11. Contract or Grant No.
	Part of DTRT13-G-UTC37

12. Sponsoring Organization Name and Address		13. Type of Report and Period Covered
Midwest Transportation Center 2711 S. Loop Drive, Suite 4700 Ames, IA 50010-8664	U.S. Department of Transportation Office of the Assistant Secretary for Research and Technology 1200 New Jersey Avenue, SE Washington, DC 20590	Final Report
		14. Sponsoring Agency Code

15. Supplementary Notes
Visit www.intrans.iastate.edu for color pdfs of this and other research reports.

16. Abstract

Current technology in traffic control is limited to a centralized approach that has not paid appropriate attention to efficiency of fuel consumption and is subject to the scale of transportation networks. This project proposes a transformative approach to the development of a distributed framework to reduce fuel consumption and travel time through the management of dynamic speed limit signs. The project proposes to integrate the roadway infrastructures equipped with sensing, communication, and parallel computation functionalities in the new traffic control paradigm.

The research approach was built on three essential objectives to establish an energy-efficient traffic control methodology:

- Implementation of a distributed control framework in large-scale transportation networks

- Simulation of dynamic traffic flow and performance tracking under implemented control signals using real-time traffic and vehicle data

- Data analysis and sustained strategy improvement

Going beyond the existing distributed architectures where precise dynamic flow models and fuel consumptions have not been considered, the work generated traffic control strategies to realize real-time, macroscopic-level traffic regulation with high precision.

Simulation results demonstrated reduced fuel consumption and alleviated traffic congestion. The feasibility of the proposed optimization method was verified through Vissim simulation that considered different traffic volumes and random seed parameters.

17. Key Words	18. Distribution Statement
fuel consumption—fuel-efficient traffic control—real-time traffic control—traffic flow simulation—transportation networks—travel time—Vissim	No restrictions.

19. Security Classification (of this report)	20. Security Classification (of this page)	21. No. of Pages	22. Price
Unclassified.	Unclassified.	43	NA

Form DOT F 1700.7 (8-72)   **Reproduction of completed page authorized**

DISTRIBUTED TRAFFIC CONTROL FOR REDUCED FUEL CONSUMPTION AND TRAVEL TIME IN TRANSPORTATION NETWORKS

Final Report
April 2018

Principal Investigator
Ran Dai, Assistant Professor
Department of Aerospace Engineering, Iowa State University

Co-Principal Investigators
Jing Dong, Transportation Engineer
Anuj Sharma, Research Scientist
Center for Transportation Research and Education, Iowa State University

Research Assistants
Yue Zu and Chenhui Liu

Authors
Yue Zu, Chenhui Liu, Ran Dai, Anuj Sharma, and Jing Dong

A report from
Institute for Transportation
Iowa State University
2711 South Loop Drive, Suite 4700
Ames, IA 50010-8664
Phone: 515-294-8103 / Fax: 515-294-0467
www.intrans.iastate.edu

TABLE OF CONTENTS

LIST OF FIGURES

LIST OF TABLES

ACKNOWLEDGMENTS

EXECUTIVE SUMMARY

This project focused on managing dynamic speed limit signs (a type of highway infrastructure that helps control traffic speeds) in order to reduce total fuel consumption during a specific time period while considering traffic flow dynamics. This involved integrating a changing inflow of traffic in real-time at a series of control intervals.

To generate a traffic control model that is computationally efficient and facilitate searching for an optimal control command, the researchers aimed to formulate the optimization performance index and dynamic traffic flow model via convex functions. In this vein, the convex optimization approach generated optimal speed profiles within polynomial computational time. Furthermore, a distributed framework was constructed based on dual decomposition and the subgradient method via networked road infrastructures.

INTRODUCTION

Large-scale, complex transportation systems are some of the most indispensable infrastructures in urban and rural areas. The dramatically increasing demands of transportation service lead to traffic congestion, energy waste, and pollution, as well as safety issues. To deal with these issues, intelligent traffic management strategies that rely on advanced sensing, communication, and high-performance computation techniques are attracting researchers' attention.

Recent work in the area of intelligent transportation systems has mostly focused on modeling and reducing travel time (Daganzo 1995, Li et al. 2014a) or minimizing delay at signalized intersections (Guler et al. 2014, Sims and Dobinson 1980). If fuel consumption is considered in evaluating transportation system performance, it is necessary to analyze the effectiveness of current traffic control systems in terms of energy efficiency while guaranteeing the accomplishment of transportation tasks within a desired timeframe.

An energy-efficient transportation system aims at reducing fuel consumption and emissions (e.g., CO, NO, CH_4) through eco-driving guidance. Existing eco-driving strategies for individual driving guidance focus on training drivers' behaviors (e.g., smooth acceleration, maintaining steady speeds, and avoiding speeds that are too fast) and have been verified to improve fuel economy on the order of 5 to 20 percent (Barkenbus 2010). However, changing driver behavior is a long-term effort and static driving advice may not guarantee prominent effects in dynamic traffic environments.

Recent studies of dynamic guidance strategies through energy-efficient traffic control include adjusting signal periods at intersections on urban roads (Li and Shimamoto 2012, Ozatay et al. 2012) and controlling the on-ramp metering rate for a proper volume of additional vehicle flow to the highway mainstream (Dai et al. 2015, Pasquale et al. 2014, Zegeye et al. 2013).

Most existing eco-driving strategies have not included a dynamic traffic flow model that characterizes the evolution of traffic flow velocity and density (Alsabaan et al. 2010, Barth et al. 2011). Although a second-order macroscopic traffic flow model (METANET) has been adopted in energy-efficient traffic management, it is time consuming to find a convergent solution when a highly nonlinear traffic flow model is considered (Zegeye 2011). Speed intervals have been used to obtain an approximate solution without solving highly nonlinear dynamics, which ultimately results in accumulative errors over time (Dai et al. 2015).

The macroscopic traffic flow model was first introduced by Lighthill and Whitham in the 1950s (Lighthill and Whitham 1955) and was intensively investigated afterward. The fundamental traffic flow model is based on the continuous conservation law in the form of partial differential equations (PDEs). For example, Lighthill-Whitham-Richard (LWR) PDEs can be solved through discrete integration methods such as the forward and backward Euler method (Press et al. 1992). Traditional numerical methods used to solve LWR PDEs lead to an approximate solution due to the reduced model.

Inspired by the Barron-Jensen/Frankowska (B-J/F) solution for Hamilton-Jacobi (HJ) PDEs (Barron and Jensen 1990), the researchers adopted the B-J/F solution to Moskowitz HJ PDEs (Bayen et al. 2007, Lighthill and Whitham 1955, Richards 1956) to obtain exact solutions without approximation. The solution can be explicitly expressed based on a pre-specified fundamental diagram (Greenshields et al. 1935) associated with initial and boundary conditions. Furthermore, the solution to Moskowitz HJ PDEs can be simplified based on roadway decomposition and traffic status.

Combing the simplified solution to Mozkowitz HJ PDEs with the quadratic formulation of the Computer Programme to calculate Emissions from Road Transport (COPERT) fuel consumption model (Ntziachristos et al. 2000), the researchers formulated the energy-efficient traffic control problem as a convex quadratic optimization problem (CQOP). Furthermore, a distributed framework was constructed to circumvent the utilization of global information. Dual decomposition and the subgradient method were implemented so that each decomposed subproblem could be solved individually in an iterative manner. The road infrastructures (RIs) that integrate the functions of measuring, displaying, communication, and computation were installed at each decomposed road segment to guide drivers to travel at an optimal desired speed.

The contributions of our work are as follows:

- The work in Claudel and Bayen (2010a) and Claudel and Bayen (2010b) presents explicit solutions and model constraints using the triangular fundamental diagram associated with initial and boundary conditions. Based on that, the researchers developed an explicit solution to Moskowitz HJ PDEs and model constraints using a parabolic-shaped fundamental diagram. Moreover, a simplified model with linear constraints was proposed.

- The energy-efficient traffic control problem was formulated as a CQOP, which was computationally efficient.

- Experimental verification was accomplished in Vissim simulation environments using real-world traffic flow data on segments of I-235 in Iowa. We constructed a component object model (COM) interface to build a connection between MATLAB and the Vissim simulations. Furthermore, we present a framework of data and control flow applicable to real-time implementation.

- A distributed framework was constructed and applied optimal traffic control problems. It was supported by local RI networks that depend on local traffic information exchanges. The distributed framework significantly reduced computational complexity by decomposing a centralized optimization problem into a set of small-scale subproblems. Meanwhile, local information transmission effectively avoided missing data or redundancy.

- The above results led to two published conference papers and one journal paper under review (Dai et al. 2015, Zu et al. 2016a, Zu et al. 2016b).

PROBLEM DESCRIPTION

The one-dimensional, uniform highway section considered in this project was represented by $[\xi, \chi]$, where ξ and χ are upstream and downstream boundaries. The vehicle density was denoted as $\rho(t, x)$ per unit length for local position $x \in [\xi, \chi]$ at time $t \in [0, t_M]$. The inflow and outflow were denoted as Q_ξ and Q_χ, respectively. The vehicle velocity was a function of ρ and was denoted as $v = v(\rho(t, x))$. The goal of the proposed traffic control strategy was to minimize the fuel consumption of vehicles on the specific highway section for a desired time interval based on current traffic status by controlling dynamic speed limit signals. An example of a traffic control scenario is shown in Figure 1.

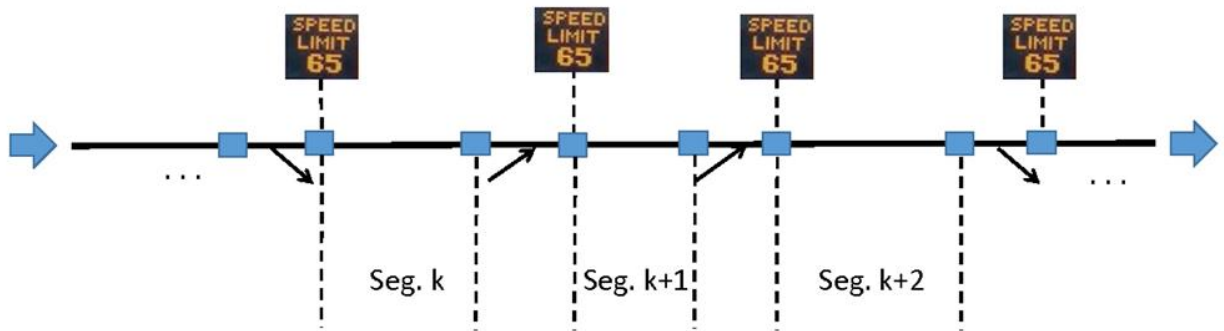**Figure 1. Sample traffic control scenario**

The arrows at the beginning and ending upstream and downstream boundaries show the vehicle flow direction, while arrows pointing off from and onto the main road section denote on-ramps and off-ramps. Rectangles outline the sensor installation locations for volume measurement, while the dynamic speed limit signs are located at the starting point of each road segment.

3

TRAFFIC FLOW DYNAMICAL MODEL

Cauchy Problem

The first order traffic flow model is known as the LWR PDE, written as follows:

$$\frac{\partial \rho}{\partial t} + \frac{\partial Q(\rho(t, x))}{\partial x} = 0 \tag{1}$$

The LWR PDE is the fundamental traffic flow model based on the continuous conservation law. By introducing the cumulated vehicle count $N(t, x)$, the vehicle density and flow could be calculated directly from the partial derivatives with respect to local position x and time t in the following forms:

$$\rho(t, x) = -\frac{\partial N(t, x)}{\partial x} \tag{2}$$

$$Q(t, x) = \frac{\partial N(t, x)}{\partial t}. \tag{3}$$

Substituting $\rho(t, x)$ and $Q(t, x)$ in Equation (1) by (2) and (3), and then integrating both sides with respect to the local position, generated the Moskowitz HJ PDE:

$$\frac{\partial N(t, x)}{\partial t} - Q(-\frac{\partial N(t, x)}{\partial x}) = 0 \tag{4}$$

Considering the initial, upstream, and downstream boundary conditions (i.e., $c_{ini}(x)$, $c_{up}(t)$, and $c_{down}(t)$) together with the Moskowitz HJ PDE, the Cauchy problem (Mazaré et al. 2011) was formulated as follows:

$$\begin{cases} (4) \\ N(0, x) = c_{ini}(x) \\ N(t, \xi) = c_{up}(t) \\ N(t, \chi) = c_{down}(t) \end{cases} \tag{5}$$

The fuel-efficient traffic control problem was to minimize fuel consumption while satisfying the four equality constraints of the Cauchy problem, listed above, by designing control variables $v(t, x)$.

Barron-Jensen/Frankowska Solution

The researchers aggregated initial, upstream, and downstream boundary conditions in a value condition function, $c(t, x)$; then, the B-J/F solution to Equation (4) could be represented as follows (Claudel and Bayen 2010a):

$$N_{\mathbf{c}}(t, x) = \inf_{(u,T)\in[w,v_f]\times\mathbb{R}_+} [\mathbf{c}(t - T, x - Tu) + TR(u)]$$

(6)

where the convex transform $R(u)$ is defined as follows:

$$R(u) = \sup_{\rho\in[0,\rho_j]} (Q(\rho) - u\rho), \ \forall u \in [w, v_f]$$

(7)

with $w = \frac{dQ}{d\rho}\big|_{\rho=\rho_j} < 0$ and $\rho_j > 0$ denoting the jam density and $v_f = \frac{dQ}{d\rho}\big|_{\rho=0} > 0$ denoting the free-flow speed. However, the solution to the HJ PDE may not be compatible with value conditions. Based on the Inf-morphism property (Claudel 2010) and Lax-Hopf formula in Equation (6), the last three equalities in the Cauchy problem could be converted into a set of inequalities.

Lemma 1 Compatibility Conditions: The solution to HJ PDE was characterized by the Inf-morphism property (Li et al. 2014b), i.e., $\mathbf{c}(t, x) = \min_{l\in L} c_l(t, x)$, where L is the index number of the value condition, the solution $\mathbf{N_c}(t, x) = \min_{l\in L} N_{c_l}(t, x)$ for $(t, x) \in [0, t_M] \times [\xi, \chi]$. The B-J/F solution to Equation (4) satisfied the value conditions when, and only when,

$$N_{c_i}(t, x) \geq c_j(t, x), \ \forall(t, x) \in Dom(c_j), \ (i, j) \in L^2$$

(8)

Inequalities in Equation (8) represent the model constraints. By considering these constraints, the B-J/F solutions were reduced to a subset representing the exact solution to the Cauchy problem. The solution to the HJ PDE could be explicitly expressed based on the Lax-Hopf formula. These expressions were integrated with piecewise affine value conditions to formulate model constraints. The researchers first defined initial and boundary conditions as explained in the following sections.

Piecewise Affine Initial and Boundary Conditions

The time period $[0, t_M]$ and highway section $[\xi, \chi]$ were discretized into several small intervals using time step T and spatial step X. The initial vehicle density, $\rho(0, x_k)$, $k = 0, \dots, k_m$, was assumed to be identical within the segment $[x_k, x_{k+1}]$. Inflow and outflow remained constant during each time interval $[t_n, t_{n+1}]$ indexed by $n = 0, \dots, n_m$. The initial and boundary

conditions, c_{ini}, c_{up} and c_{down}, can be decomposed into an affine, locally defined condition set (i.e., c_{ini}^k, c_{up}^n and c_{down}^n). For example, the negative initial condition, $-c_{ini}^k(t,x)$, represents the total number of vehicles at initial time contained between $[\xi, \chi]$. The upstream condition, $c_{up}^n(t,x)$, depicts the total number of vehicles entering the roadway from initial to current time, t. Hence, the piecewise affine equations were summarized regarding initial and boundary conditions as follows (Canepa and Claudel 2012):

$$
c_{ini}^k(t,x) = \begin{cases} -\sum_{i=0}^{k-1} \rho(0,x_i)X - \rho(0,x_k)(x - kX), \\ if \ t = 0 \ \& \ x \in [x_k, x_{k+1}] \\ +\infty, \ otherwise \end{cases}
$$

(9)

$$
c_{up}^n(t,x) = \begin{cases} \sum_{i=0}^{n-1} Q(t_i,\xi)T + Q(t_n,\xi)(t - nT), \\ if \ x = \xi \ \& \ t \in [t_n, t_{n+1}] \\ +\infty, \ otherwise \end{cases}
$$

(10)

$$
c_{down}^n(t,x) = \begin{cases} \sum_{i=0}^{n-1} Q(t_i,\chi)T + Q(t_n,\chi)(t - nT) \\ -\sum_{k=0}^{k_m} \rho(0,x_k)X, \ if \ x = \chi \ \& \ t \in [t_n, t_{n+1}] \\ +\infty. \ otherwise \end{cases}
$$

(11)

B-J/F Explicit Solution Associated with Initial and Boundary Conditions

The relationship between Q and ρ is represented by a fundamental diagram $Q(\rho)$, which is established from empirical measurements. The flow-density curve can be triangular or parabolic in shape. In this section, the researchers describe the adopted Greenshields model, which is one of the typical parabolic-shaped models. The comparison to using the triangular model is also described.

First, $Q(\rho)$ was substituted with the Greenshields flow density model in Equation (7). Since $Q(\rho) - \frac{x-x_k}{t}\rho$ is concave, the supremum can be found by satisfying the first order necessary condition. The transformed $R(\frac{x-x_k}{t})$ was explicitly expressed as follows:

$$R\left(\frac{x - x_k}{t}\right) = \frac{v_f}{4}\rho_j + \frac{(x - x_k)^2 \rho_j}{4 v_f t^2} - \frac{x - x_k}{2t}\rho_j$$

(12)

Based on the solutions to the Moskowitz function provided from Equations (21), (24), and (27), which are explained below (from Mazaré et al. 2011), Q and R were replaced by the Greenshields model and the expressions in Equation (12), respectively. The B-J/F explicit solutions were obtained as follows. The initial condition included two cases: the initially uncongested case when $0 \leq \rho(0, x) \leq \rho_c$, where ρ_c denotes the critical density,

$$N_{c_{ini}^k}(t, x) = \begin{cases} \left(-\dfrac{v_f}{\rho_j}\rho(0, x_k)^2 + v_f\rho(0, x_k)\right)t + c_{ini}^k(0, x), \\ \quad if\ \dfrac{x - x_{k+1}}{Q'(\rho_k)} \leq t \leq \dfrac{x - x_k}{Q'(\rho_k)} \\ \dfrac{v_f}{4}\rho_j t + \dfrac{(x - x_k)^2 \rho_j}{4 v_f t} - \dfrac{x - x_k}{2}\rho_j + c_{ini}^k(0, x_k), \\ \quad if\ t \geq \dfrac{x - x_k}{Q'(\rho_k)} \end{cases}$$

(13)

and the initially congested case when $\rho_c \leq \rho(0, x) \leq \rho_j$,

$$N_{c_{ini}^k}(t, x) = \begin{cases} \left(-\dfrac{v_f}{\rho_j}\rho(0, x_k)^2 + v_f\rho(0, x_k)\right)t + c_{ini}^k(0, x), \\ \quad if\ \dfrac{x - x_k}{Q'(\rho_k)} \leq t \leq \dfrac{x - x_{k+1}}{Q'(\rho_k)} \\ \dfrac{v_f}{4}\rho_j t + \dfrac{(x - x_{k+1})^2 \rho_j}{4 v_f t} - \dfrac{x - x_{k+1}}{2}\rho_j + c_{ini}^k(0, x_{k+1}), \\ \quad if\ t \geq \dfrac{x - x_{k+1}}{Q'(\rho_k)} \end{cases}$$

(14)

where $Q'(\rho_k) = \dfrac{dQ(\rho)}{d\rho}\big|_{\rho = \rho(0, x_k)}$. For the upstream boundary condition, the corresponding explicit solution based on the Lax-Hopf formula was as follows:

$$
N_{c_{up}^n}(t,x) = \begin{cases}
\dfrac{(v_f - \frac{x-\xi}{t-t_n})^2 \rho_j}{4v_f}(t-t_n) + c_{up}^n(t_n,\xi), \\[4pt]
\quad if\ t_n \le t \le t_n + T_0(\rho_{up}) \\[4pt]
-\rho_{up}(x-\xi) + c_{up}^n(t,x), \\[4pt]
\quad if\ t_n + T_0(\rho_{up}) \le t \le t_{n+1} + T_0(\rho_{up}) \\[4pt]
(v_f - \dfrac{x-\xi}{t-t_{n+1}})^2 \rho_j(t-t_{n+1})/4v_f + c_{up}^n(t_{n+1},\xi), \\[4pt]
\quad if\ t \ge t_{n+1} + T_0(\rho_{up})
\end{cases}
\tag{15}
$$

For the downstream boundary condition, the corresponding explicit solution based on the Lax-Hopf formula was as follows:

$$
N_{c_{down}^n}(t,x) = \begin{cases}
\dfrac{(v_f - \frac{\chi-x}{t_n-t})^2 \rho_j}{4v_f}(t-t_n) + c_{down}^n(t_n,\chi), \\[4pt]
\quad if\ t_n \le t \le t_n + T_0(\rho_{down}) \\[4pt]
\rho_{down}(\chi-x) + c_{down}^n(t,x), \\[4pt]
\quad if\ t_n + T_0(\rho_{down}) \le t \le t_{n+1} + T_0(\rho_{down}) \\[4pt]
(v_f - \dfrac{\chi-x}{t_{n+1}-t})^2 \rho_j(t-t_{n+1})/4v_f + c_{down}^n(t_{n+1},\chi), \\[4pt]
\quad if\ t \ge t_{n+1} + T_0(\rho_{down})
\end{cases}
\tag{16}
$$

where $T_0(\rho_{up}) = \frac{x-\xi}{Q'(\rho_{up})}$, $T_0(\rho_{down}) = \frac{x-\chi}{Q'(\rho_{down})}$, $\rho_{up} = \min\{\rho \in [0,\rho_j] | Q(\rho) = Q(t,\xi)\}$, and $\rho_{down} = \max\{\rho \in [0,\rho_j] | Q(\rho) = Q(t,\chi)\}$. In the next section, the researchers discuss the simplified form of Equations (13) through (16) for cases with relatively large traffic inflow and outflow.

Simplified B-J/F Solution

Assumption 1. A one-lane highway with a relatively long distance can be decomposed into several segments with identical distances of X for each segment. The B-J/F solution can then be implemented in each of these segments.

Assumption 2. The highway section is required to handle cases with relatively large vehicle flows (i.e., flow at origin and ending close to road capacity Q_c). In other words, the section has $\left(1 - \frac{1}{\sqrt{q}}\right)\rho_c \le \rho_{up} \le \rho_c$ and $\rho_c \le \rho_{down} \le \left(1 + \frac{1}{\sqrt{q}}\right)\rho_c$, where q is a user-specified parameter determining the bounds of constraints. Substituting the above bounds on ρ_{up} and ρ_{down} in the

$T_0(\rho_{up})$ and $T_0(\rho_{down})$ expressions, respectively, yields $T_0(\rho_{up}) \geq \sqrt{q}\frac{x-\xi}{v_f}$ and $T_0(\rho_{down}) \geq \sqrt{q}\frac{x-x}{v_f}$.

Each road segment is regarded as an individual object with associated length, X, jam density, ρ_j, and free-flow speed, v_f, after decomposition. To make it simple, we used the same notation X, ρ_j, and v_f in the simplified B-J/F solution.

Assumption 1 simply sets the initial density to be $\rho(0,0)$, $\rho(0,X)$, and denotes $\rho_{ini} = \rho(0,0)$ as vehicle density for each segment. To simplify the representation, ρ_{ini} was used for different segments in the following derivation. Furthermore, the plot of the function in Equation (15) in Figure 2 demonstrates that the slope of tangent line at each time instance increased when t varied from $t_n + \frac{x-\xi}{v_f}$ to $\frac{v_f\rho_j}{4}$.
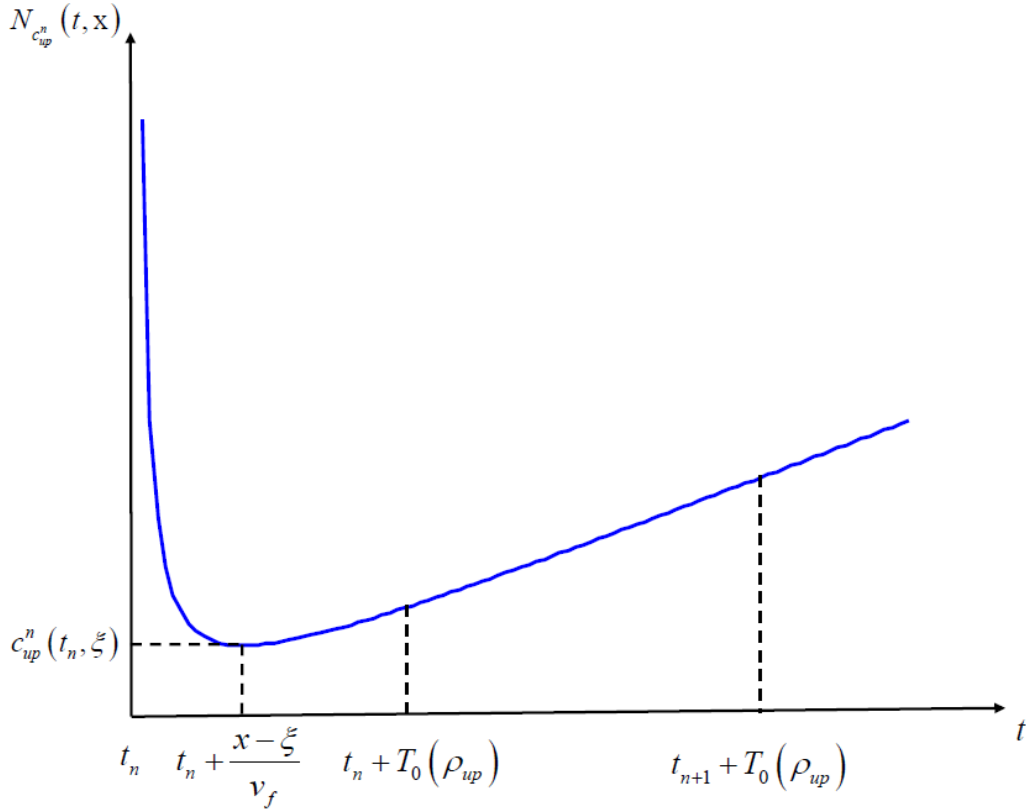

Figure 2. Sketch of function shown in Equation (15)

Similar conclusions can be derived from the solution curve associated with the downstream boundary condition. Assumption 2 introduces a linear approximation for Equations (15) and (16) when $t \geq \sqrt{q}\frac{X}{v_f}$. Based on these discussions, the initial and boundary conditions for each road

segment, with modified notations of $Q_{up}^t = Q(t, 0)$, $Q_{up}^t = Q(t, X)$, and ρ_{ini} are expressed as follows:

$$c_{ini}^0(t, x) = \begin{cases} -\rho_{ini}x, & if\ t = 0\ \&\ x \in [0, X] \\ +\infty, & otherwise \end{cases} \tag{17}$$

$$c_{up}^n(t, x) = \begin{cases} \sum_{i=0}^{n-1} Q_{up}^{t_i} T + Q_{up}^{t_n}(t - nT), \\ if\ x = 0\ \&\ t \in [t_n, t_{n+1}] \\ +\infty,\ otherwise \end{cases} \tag{18}$$

$$c_{down}^n(t, x) = \begin{cases} \sum_{i=0}^{n-1} Q_{down}^{t_i} T + Q_{down}^{t_n}(t - nT) \\ -\rho_{ini}X,\ if\ x = X\ \&\ t \in [t_n, t_{n+1}] \\ +\infty,\ otherwise. \end{cases} \tag{19}$$

With the updated initial and boundary conditions, the B-J/F solution associated with the initial condition was simplified. For the initially free-flow case, with $0 \leq \rho_{ini} \leq \rho_c$, the solution reduces to the following:

$$N_{c_{ini}^0}(t, x) = \begin{cases} (-\dfrac{v_f}{\rho_j}\rho_{ini}^2 + v_f\rho_{ini})t - \rho_{ini}x, \\ if\ 0 \leq t \leq \dfrac{x}{Q'(\rho_{ini})} \\ \dfrac{v_f}{4}\rho_j t + \dfrac{x^2\rho_j}{4v_f t} - \dfrac{x}{2}\rho_j, \\ if\ t \geq \dfrac{x}{Q'(\rho_{ini})} \end{cases} \tag{20}$$

For the initially congested case, with $\rho_c \leq \rho_{ini} \leq \rho_j$, the solution becomes the following:

$$
N_{c_{ini}^0}(t,x) = \begin{cases} (-\dfrac{v_f}{\rho_j}\rho_{ini}^2 + v_f\rho_{ini})t - \rho_{ini}x, \\[4pt] \quad if\ 0 \le t \le \dfrac{x - X}{Q'(\rho_{ini})} \\[6pt] \dfrac{v_f}{4}\rho_j t + \dfrac{(x - X)^2\rho_j}{4v_f t} - \dfrac{x - X}{2}\rho_j - \rho_{ini}X, \\[6pt] \quad if\ t \ge \dfrac{x - X}{Q'(\rho_{ini})} \end{cases}
$$

(21)

The solution components associated with boundary conditions become the following:

$$
N_{c_{up}^n}(t,x) = \begin{cases} \dfrac{(v_f - \frac{x}{t-t_n})^2\rho_j}{4v_f}(t - t_n) + \displaystyle\sum_{i=0}^{n-1} Q_{up}^{t_i}T, \\[6pt] \quad if\ t_n \le t \le t_n + \sqrt{q}\dfrac{x}{v_f} \\[6pt] a(t - t_n) + b, \quad if\ t \ge t_n + \sqrt{q}\dfrac{x}{v_f} \end{cases}
$$

(22)

$$
N_{c_{down}^n}(t,x) = \begin{cases} \dfrac{(v_f - \frac{X-x}{t_n-t})^2\rho_j}{4v_f}(t - t_n) + \displaystyle\sum_{i=0}^{n-1} Q_{down}^{t_i}T - \rho_{ini}X, \\[6pt] \quad if\ t_n \le t \le t_n + \sqrt{q}\dfrac{X - x}{v_f} \\[6pt] e(t - t_n) + f, \quad if\ t \ge t_n + \sqrt{q}\dfrac{X - x}{v_f} \end{cases}
$$

(23)

where a, e are slopes of the tangent line at the corresponding time and b, f are the relative function values at $t = t_n + \sqrt{q}\dfrac{x}{v_f}$ and $t = t_n + \sqrt{q}\dfrac{X-x}{v_f}$.

Model Constraints

As described above, the B-J/F solution is an exact solution to the Cauchy problem if the inequality of Equation (8) holds. The researchers reduced these continuous inequalities for $\forall(t,x) \in Dom(c_j)$ into a series of discrete inequalities by discretizing the continuous time interval into a set of small time intervals with step size T = 1 sec. By utilizing the linear interpolation on [pT, (p+1)T], the piecewise affine functions were built with respect to time, t. Therefore, the discrete inequality constraints are expressed as follows:

$$
\begin{cases}
(i) \ N_{c_{up}^n}(0,x) \geq c_{ini}^k(0,x), \\
\qquad \forall (n,k) \in \{0,...,n_m\} \times \{0,...,k_m\} \ \& \ x \in [kX,(k+1)X] \\
(ii) \ N_{c_{ini}^k}(t,\xi) \geq c_{up}^p(t,\xi) \\
\qquad \forall (k,p) \in \{0,...,k_m\} \times \{0,...,n_m\} \ \& \ t \in [pT,(p+1)T] \\
(iii) \ N_{c_{down}^n}(0,x) \geq c_{ini}^k(0,x) \\
\qquad \forall (n,k) \in \{0,...,n_m\} \times \{0,...,k_m\} \ \& \ x \in [kX,(k+1)X] \\
(iv) \ N_{c_{ini}^k}(t,\chi) \geq c_{down}^p(t,\chi) \\
\qquad \forall (k,p) \in \{0,...,k_m\} \times \{0,...,n_m\} \ \& \ t \in [pT,(p+1)T] \\
(v) \ N_{c_{up}^n}(t,\chi) \geq c_{down}^p(t,\chi) \\
\qquad \forall (n,p) \in \{0,...,n_m\}^2 \ \& \ t \in [pT,(p+1)T] \\
(vi) \ N_{c_{down}^n}(t,\xi) \geq c_{up}^p(t,\xi) \\
\qquad \forall (n,p) \in \{0,...,n_m\}^2 \ \& \ t \in [pT,(p+1)T]
\end{cases}
\tag{24}
$$

Constraints (i) and (iii) in Equation (24) were satisfied for $x \in [\xi,\chi]$, $t \in [0,t_M]$ in the simplified solution (Claudel and Bayen 2010a). The remaining constraints in Equation (24) were replaced by corresponding expressions defined in Equations (17) through (23). For an initially free-flow condition, with $\rho_{ini} \leq \rho\_c$, and a discrete time index or $\rho \in [n,n_m]$ for $t \in [pT,(p+1)T]$, constraints (ii) and (iv) in Equation (24) become the following:

$$
(ii) \quad \frac{v_f \rho_j}{4}t \geq Q_{up}^{t_p}(t-pT) + \sum_{l=0}^{p-1} Q_{up}^{t_l}T
\tag{25}
$$

$$
(iv)
\begin{cases}
(-\dfrac{v_f}{\rho_j}\rho_{ini}^2 + v_f \rho_{ini})t \geq Q_{down}^{t_p}(t-pT) + \displaystyle\sum_{l=0}^{p-1} Q_{down}^{t_l}T, \ if \ 0 \leq t \leq \dfrac{X}{Q'(\rho_{ini})} \\[4mm]
(\dfrac{v_f \rho_j}{4} - Q_{down}^{t_p})t^2 + (Q_{down}^{t_p}pT - \displaystyle\sum_{l=0}^{p-1} Q_{down}^{t_l}T + (\rho_{ini} - \dfrac{\rho_j}{2})X)t \\[4mm]
+ \dfrac{X^2 \rho_j}{4v_f} \geq 0, \ if \ t \geq \dfrac{X}{Q'(\rho_{ini})}.
\end{cases}
\tag{26}
$$

For initially congested conditions with $\rho_{ini} \geq \rho_c$, constraints (ii) and (iv) in Equation (24) become the following:

$$(ii) \begin{cases} (-\dfrac{v_f}{\rho_j}\rho_{ini}^2 + v_f\rho_{ini})t \geq Q_{up}^{t_p}(t - pT) + \sum_{l=0}^{p-1} Q_{up}^{t_l}T, \\[2mm] \quad if \ 0 \leq t \leq \dfrac{-X}{Q'(\rho_{ini})} \\[2mm] (\dfrac{v_f\rho_j}{4} - Q_{up}^{t_p})t^2 + (Q_{up}^{t_p}pT - \sum_{l=0}^{p-1} Q_{up}^{t_l}T + (\rho_{ini} - \dfrac{\rho_j}{2})X)t \\[2mm] \quad + \dfrac{X^2\rho_j}{4v_f} \geq 0, \ if \ t \geq \dfrac{-X}{Q'(\rho_{ini})}, \end{cases}$$

$$(27)$$

$$(iv) \ \dfrac{v_f\rho_j}{4}t \geq Q_{down}^{t_p}(t - pT) + \sum_{l=0}^{p-1} Q_{down}^{t_l}T.$$

$$(28)$$

For $t_n \leq t \leq t_n + \sqrt{q}\dfrac{X}{v_f}$, constraints (v) and (vi) in Equation (24) become the following:

$$(v)(\dfrac{v_f\rho_j}{4} - Q_{down}^{t_p})(t - nT)^2 + (W + Q_{down}^{t_p}(p - n)T - \sum_{l=n}^{p-1} Q_{down}^{t_l}T)(t - nT) + \dfrac{X^2\rho_j}{4v_f} \geq 0,$$

$$(29)$$

$$(vi)(\dfrac{v_f\rho_j}{4} - Q_{up}^{t_p})(t - nT)^2 + (-W + Q_{up}^{t_p}(p - n)T - \sum_{l=n}^{p-1} Q_{up}^{t_l}T)(t - nT) + \dfrac{X^2\rho_j}{4v_f} \geq 0,$$

$$(30)$$

where $W = \sum_{t=0}^{n-1}(Q_{up}^{t_l} - Q_{down}^{t_l})T + (\rho_{ini} - \dfrac{\rho_j}{2})X$. For $t \geq t_n + \sqrt{q}\dfrac{X}{v_f}$, constraints (v) and (vi) in Equation (24) become the following:

$$(v)(a - Q_{down}^{t_p})(t - nT) + Q_{down}^{t_p}(p - n)T + \rho_{ini}X + b - \sum_{l=0}^{p-1} Q_{down}^{t_l}T \geq 0,$$

$$(31)$$

$$(vi)(e - Q_{up}^{t_p})(t - nT) + Q_{up}^{t_p}(p - n)T + f - \sum_{l=0}^{p-1} Q_{up}^{t_l}T \geq 0.$$

$$(32)$$

Expressions in Equation (24) are model constraints describing traffic flow dynamics. Constraints shown in Equations (25) and (28) have been verified in Claudel and Bayen (2010a) because $\dfrac{v_f\rho_j}{4} \geq max_{t\in[0,t_M]}\{Q_{up}^t, Q_{down}^t\}$. Hence, both of these constraints are ignored in the formulation of the optimization problem described in the following chapter.

13

FUEL CONSUMPTION MODEL

The COPERT model is a macroscopic model that estimates the emission and fuel consumption rate based on average vehicle speed (Zegeye 2011). The quadratic form of emission or fuel consumption with respect to average speed ,v_a, is expressed as follows:

$$J = c_0 v_a^2 + c_1 v_a + c_2,$$

(33)

where c_0, c_1, and c_2 are parameters specified in terms of vehicle categories such as passenger cars, light-duty vehicles, and heavy-duty vehicles. The researchers defined average vehicle speed at time t and location x as $v_a(t,x) = \{v_a(t,x) \in [0, v_f]\}$. From the Greenshields fundamental diagram, $v_a = \frac{Q(\rho_a)}{\rho_a} = -\frac{v_f}{\rho_j}\rho_a(t,x) + v_f$, where $\rho_a(t,x) = \frac{(Q_{up}^{(t,x)} - Q_{down}^{(t,x)})T + \rho(t,x)}{X}$ is the average vehicle density.

Assuming vehicles belong to the EURO I class, the speed range is 13.1 km/h (8 mph) to 130 km/h (81 mph), with a cylinder capacity range of 1.41 to 2.01 L for each vehicle, and the performance index is then based on a fuel consumption rate in g/km, which is constructed as follows:

$$
\begin{aligned}
J &= \sum_{k=0}^{k_m} X^k [c_0 v_a(t_{n+1}, x_k)^2 + c_1 v_a(t_{n+1}, x_k) + c_2] \\
&= \sum_{k=0}^{k_m} X^k [c_0(-\frac{v_f^k}{\rho_j^k}\rho_a(t_{n+1}, x_k) + v_f^k)^2 + c_1(-\frac{v_f^k}{\rho_j^k}\rho_a(t_{n+1}, x_k) + v_f^k) + c_2] \\
&= \sum_{k=0}^{k_m} X^k [c_0(-\frac{v_f^k}{\rho_j^k}\frac{(Q_{up}^{(t_n, x_k)} - Q_{down}^{(t_n, x_k)})T + \rho(t_n, x_k)X^k}{X^k} + v_f^k)^2 \\
&\quad + c_1(-\frac{v_f^k}{\rho_j^k}\frac{(Q_{up}^{(t_n, x_k)} - Q_{down}^{(t_n, x_k)})T + \rho(t_n, x_k)X^k}{X^k} + v_f^k) + c_2]
\end{aligned}
$$

(34)

where the superscript of X^k, v_f^k, and ρ_j^k denotes the segment index k. The quadratic form of the objective function is determined by $Q_{up}^{(t_n, x_k)}$ and $Q_{down}^{(t_n, x_k)}$. The performance index in Equation (34) denotes the fuel consumed on road section $[\xi, \chi]$ during the time interval $[t_{n+1}, t_{n+2}]$, given the density of $\rho(t_n, x_k)$. Moreover, the Hessian matrix of the above objective function in Equation (34) is expressed as follows:

$$H = \begin{bmatrix} p^0 & -p^0 & 0 & 0 & \dots & 0 \\ -p^0 & p^0 & 0 & 0 & \dots & 0 \\ 0 & 0 & p^1 & -p^1 & \dots & 0 \\ 0 & 0 & -p^1 & p^1 & \dots & 0 \\ \dots & \dots & \dots & \dots & \dots & \dots \\ 0 & \dots & 0 & 0 & p^{k_m} & -p^{k_m} \\ 0 & \dots & 0 & 0 & -p^{k_m} & p^{k_m} \end{bmatrix}$$

(35)

with $p^k = 2c_0 \left(\frac{v_f^k}{\rho_j^k} \frac{T}{X^k} \right)^2$, as positive semi-definite, which implies a convex objective function.

FORMULATION OF CONVEX OPTIMIZATION PROBLEM

For this project, the additional traffic inflow and outflow from on-ramp and off-ramp traffic were considered. The volume on each off-ramp was assumed to be proportional to the corresponding main highway section volume with a constant ratio of $R_{off}^{x_k}$, while the on-ramp vehicle volume was assumed constant, as denoted by $C_{on}^{x_k}$. Thus, additional linear equality constraints related to inflow and outflow were included in the problem formulation. Considering both ramp-effect constraints and the linear model constraints in terms of $Q_{up}^{(t_n,x_k)}$ and $Q_{down}^{(t_n,x_k)}$, the fuel-efficient traffic control problem was formulated as follows:

$$
\begin{aligned}
\min. \quad & J = \qquad (34)\\
s.t. \quad & A_{model}\mathbf{y} \leq b_{model}\\
& Q_{down}^{(t_n,x_k)} = Q_{up}^{(t_n,x_{k+1})}, \ k = 0,...,k_m - 1, \ \text{if no ramp exists on } [x_k, x_{k+1}]\\
& (1 - R_{off}^{x_k})Q_{down}^{(t_n,x_k)} = Q_{up}^{(t_n,x_{k+1})}, \ k = 0,...,k_m - 1, \ \text{if off-ramp exists on } [x_k, x_{k+1}]\\
& Q_{down}^{(t_n,x_k)} + C_{on}^{x_k} = Q_{up}^{(t_n,x_{k+1})}, \ k = 0,...,k_m - 1, \ \text{if on-ramp exists on } [x_k, x_{k+1}],
\end{aligned}
$$

$$(36)$$

where A_{model} and b_{model} represent the parameter matrix and vector derived from the linear model constraints in Equations (25) through (32). The unknown variable set,

$$
\mathbf{y} = [Q_{down}^{(t_n,x_0)}, \ Q_{up}^{(t_n,x_0)}, \ ..., \ Q_{down}^{(t_n,x_{k_m})}, \ Q_{up}^{(t_n,x_{k_m})}]^T,
$$

$$(37)$$

includes traffic inflow and outflow at the time instant (t_n) for all segments.

By solving the above problem in the form of the CQOP, the researchers found the optimized traffic inflow and outflow variables for each segment during $[t_n, t_{n+1}]$. From the determined $Q_{up}^{(t_n,x_k)}$ and $Q_{down}^{(t_n,x_k)}$ for $k = 0, ... , k_m$, the desired vehicle density for the next time interval could then be obtained from the following:

$$
\rho(t_{n+1}, x_k) = \frac{(Q_{up}^{(t_n,x_k)} - Q_{down}^{(t_n,x_k)})T + \rho(t_n, x_k)X^k}{X^k},
$$

$$(38)$$

which was based on the cell-transmission model (Daganzo 1994). To reach the desired vehicle density at the next time instant, t_{n+1}, the desired speed of each segment at the time interval shown as $[t_n, t_{n+1}]$ was determined by the following:

$$v_d(t_n, x_k) = -\frac{v_f^k}{\rho_j^k}\rho(t_{n+1}, x_k) + v_f^k.$$

(39)

From Equation (39), optimized traffic inflow and outflow decision variables were then converted into the desired speed for segment k during $[t_n, t_{n+1}]$, which was the control variable set expressed as follows:

$$\mathbf{v} = [v_d(t_n, x_0),\ v_d(t_n, x_1),\ ...,\ v_d(t_n, x_{k_m})]^T.$$

(40)

DUAL DECOMPOSITION AND SUBGRADIENT METHOD

Layout of Distributed Road Infrastructure Network

The formulated problem described above required that data be collected from both on-ramp and off-ramp vehicle volumes for controlled segments and sent to a central processor. Instead of solving the traffic control problem in a central processor, which requires communication with each volume sensor, a distributed traffic control network was proposed.

The traffic control network, equipped with sensing, computation, traffic information transmission, and display panels, is illustrated in Figure 3.
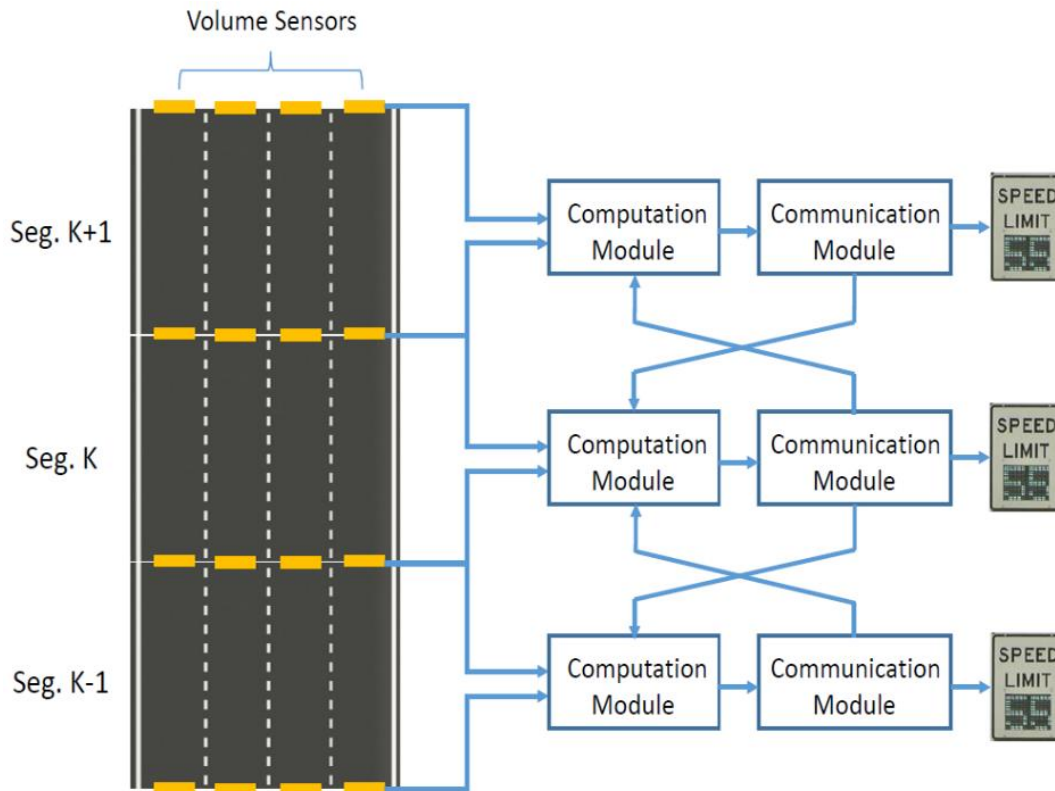
Figure 3. Road infrastructure components and information flow

The volume sensors count the number of vehicles entering and exiting segment K during time interval $[t_{n-1}, t_n]$. The computation module calculates instantaneous vehicle density at t_n and handles it as the initial state for the next time interval, $[t_n, t_{n+1}]$. Based on obtained initial density, CQOPs are solved using QP individually. Temporary optimal solutions y_k^* are transmitted to adjacent RIs through a communication module. Subproblem formulation is then updated and CQOPs are resolved. This procedure was repeated until the ramp-effect constraints in Equation (36) were satisfied for all $k \in \{0, \dots, k_m - 1\}$. The converged solution for traffic inflow and outflow was transferred to the desired velocity using Equations (38) and (39). The

optimal speed of the dynamic limit signs at t_n was updated to guide drivers during the time interval $[t_n, t_{n+1}]$.

The RIs in the network compute desired speed for the corresponding segment in a distributed manner. In order to satisfy the ramp-effect constraints, each computation module exchanges information concerning optimized traffic flow only with neighboring segments. Compared to the centralized algorithm, which solves the entire problem in one computation module, decomposed subproblems at a small scale can be solved by individual computation modules. Furthermore, the distributed framework effectively prevents failure due to damage or breakdown of any RIs. Meanwhile, parallel computation of subproblems improves the entire system's efficiency.

Dual Decomposition

The researchers first constructed the Lagrangian by introducing multipliers λ_k associated with ramp-effect constraints from Equation (36), as follows:

$$L = \sum_{k=0}^{k_m} J_k(\mathbf{y}_k) + \sum_{k=0}^{k_m-1} \lambda_k [(1 - \delta_k R_{off}^{x_k}) Q_{down}^{(t_n, x_k)} - Q_{up}^{(t_n, x_k)}]$$

(41)

where $y_k = \left[Q_{down}^{(t_n, x_k)}, Q_{up}^{(t_n, x_k)} \right]^T$. By sorting y_k in Equation (41), the Lagrangian could be rewritten as follows:

$$L = \sum_{k=0}^{k_m} [J_k(\mathbf{y}_k) + \bar{\lambda}_k^T \mathbf{y}_k].$$

(42)

where

$$\bar{\lambda}_k = \begin{cases} [(1 - \delta_k R_{off}^{x_k})\lambda_k, \ 0]^T, \ if \ k = 0 \\ [(1 - \delta_k R_{off}^{x_k})\lambda_k, \ -\lambda_{k-1}]^T, \ if \ k = 1, \ldots, k_m - 1 \\ [0, \ -\lambda_{k-1}]^T, \ if \ k = k_m \end{cases}$$

(43)

and

$$\delta_k = \begin{cases} 1, \ \text{if off-ramp exists on } [x_k, x_{k+1}], \\ \\ 0, \ \text{if no ramp or on-ramp exists on } [x_k, x_{k+1}], \end{cases}$$

(44)

Equation (42) is composed of k_m subproblems, and each is formulated as a CQOP in the following form:

$$\min_{\mathbf{y}_k} \quad J_k(\mathbf{y}_k) + \bar{\lambda}_k^T \mathbf{y}_k, \ k = 0, \ldots, k_m$$
$$s.t. \quad A_{model}^k \mathbf{y}_k \leq b_{model}^k, \tag{45}$$

where $A_{model}^k y_k \leq b_{model}^k$ represents the compact form of the dynamical constraints for subproblem k. By integrating the ramp-effect constraints in the objective function, the remaining constraints are the dynamical constraints in the formulation shown in Equation (45). Given that dynamical constraints of individual segments are only relevant to local decision variables (i.e., traffic inflow and outflow at starting and exiting points), every subproblem is independent of each other. Through the above transformation, the original optimization problem was decomposed into a set of subproblems. Thus, an optimal solution for each subproblem could be obtained individually.

Subgradient Method

The subgradient method is an iterative procedure used to gradually approach the optimal solution by finding the ascent direction for the dual problem. Given Lagrangian multipliers $\lambda_k(j)$ at iteration j, the subgradient at this point is denoted as follows:

$$h_k(j) = \begin{cases} Q_{down}^{(t_n,x_k)} - Q_{up}^{(t_n,x_k)}, & \text{if no ramp exists on } [x_k, x_{k+1}], \\ (1 - \delta_k R_{off}^{x_k}) Q_{down}^{(t_n,x_k)} - Q_{up}^{(t_n,x_k)}, & \text{if off-ramp exists on } [x_k, x_{k+1}], \\ Q_{down}^{(t_n,x_k)} - Q_{up}^{(t_n,x_k)} + C_{in}^{x_k}, & \text{if on-ramp exists on } [x_k, x_{k+1}]. \end{cases} \tag{46}$$

The Lagrangian multiplier is updated by the following:

$$\lambda_k(j + 1) = \lambda_k(j) + \alpha_k(j) h_k(j), \tag{47}$$

where $\alpha_k(j)$ is the user-specified step size that determines the convergence speed. Adjusting the step size during the coordination was challenging. On the one hand, an overly weighted step size leads to divergent results. On the other hand, too small of a step size slows the convergence speed in real-time application.

The optimal solution was to update by solving Equation (45). The procedure was repeated until $\lambda_k(j + 1) = \lambda_k(j)$. Practically, the stopping criterion for convergence was set as $|\lambda_k(j + 1) - \lambda_k(j)| < \varepsilon_\lambda$, where ε_λ was a user-specified threshold. Pseudo code for the iterative procedure is provided in the algorithm in Protocol 1.

Protocol 1. Dual Decomposition and Subgradient Method for the Distributed Traffic Control Problem

Initialization: For subproblem $k, \lambda_k(0) = 0, \lambda_k(1) = inf, j = 0$

while $|\lambda_k(j+1) - \lambda_k(j)| < \varepsilon_\lambda$ **do:**
    $j = j + 1$.
    Solve CQOP in Equation (45) to obtain $y_k(j) = [Q_{down}^{(t_n, x_k)}, Q_{up}^{(t_n, x_k)}]$.
    Calculate subgradient via Equation (46).
    Update Lagrangian multipliers via Equation (47).
end

In comparison to the centralized algorithm, optimal solutions at iteration j were exchanged with neighboring RIs to update $\lambda_k(j+1)$. The distributed algorithm did not rely on global information, which depends on a fully connected RI network. Hence, the distributed method was more efficient and easier to implement than the centralized method. Moreover, each subproblem could be solved in parallel, which reduced the overall calculation time.

SIMULATION EXPERIMENTS

Real-World Scenario and Vissim Setup

This chapter describes the implementation of the formulated CQOP to minimize fuel consumption of a 4.6 mile (7.42 km) long spatial domain of I-235 from 50th Street to Exit 5B, which is one of the busiest freeways in West Des Moines, Iowa. The existing Iowa Department of Transportation (DOT) Wavetronix sensors, which are used to capture traffic data, cover the highway network of West Des Moines and Des Moines. The collected aggregated data were obtained through an online data portal maintained by TransCore.

The weekday data for the peak morning traffic hours (7:00 am to 9:00 am) from May 1 to September 30, 2015 were used in this work. Based on the Greenshields model, linear regression was used to fit the speed-density line illustrated in Figure 4, where one example fitting line for the highway section from Valley West Drive northbound (NB) to Exit 2 is shown.

The figure shows a scatter plot with Speed [mph] on the y-axis (0 to 90) and Density on the x-axis (0 to 80). The regression equation is shown as:

$$y = -0.8775x + 81.378$$
$$R^2 = 0.8431$$

Arrows point to the Upper bound, Linear Regression, and Lower bound lines.
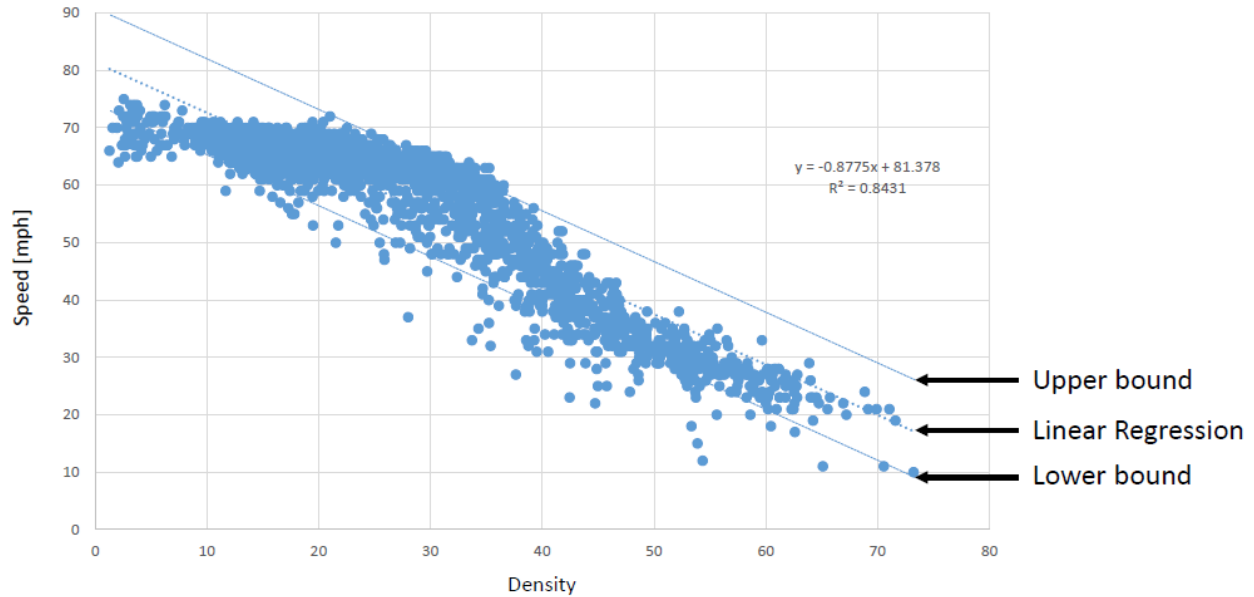
Figure 4. Speed-density line fitted through linear regression for Valley West Drive NB to Exit 2 on I-235

The corresponding parameters of the fundamental diagram were calculated graphically. By making the speed equal to zero, jam density ρ_j^k could be derived accordingly. Similarly, the free flow speed, v_f^k, was obtained by assuming the density to be zero.

The proposed traffic control strategy, by solving the formulated CQOP, was originally programmed in MATLAB. To build the connection between the control program and the Vissim simulation, the researchers generated a COM interface. The COM interface was designed to access all network object attributes and realize the user-defined control algorithms (PTV AG

2014). Through the COM interface, most of the simulation parameters could be dynamically handled during programming (Lu et al. 2012, Tettamanti and Varga 2012).

According to the ramp location, the experimental highway section is divided into 10 segments. For example, Segment 4 is shown in Figure 5.

©2016 Google

Figure 5. Segment 4: I-235 from Valley West Drive NB to Exit 2

The arrows in Figure 5 point to the locations of the volume sensors. The two blue elliptical regions at each end of the segment show the entry and exit locations for on-ramp and off-ramp vehicles, while the dynamic speed limit sign for 65 mph is shown located at the beginning of the segment on the left.

Four sensors were installed at the starting point of Segment 4, each recording traffic volume entering Segment 4 for the corresponding lane. An additional four volume sensors were installed at the ending point of Segment 4 to collect the traffic volume leaving the segment. The volume records returned to zero every 120 seconds.

The dynamic speed limit signs were located in accordance with the physical characteristics of each highway segment. For example, the sign at the starting point of Segment 4 is located right after the on-ramp of I-235 eastbound (EB) at Valley West Drive NB, as shown in Figure 5. Each highway segment had only one speed limit sign, and its location overlapped with the starting point of the segment, which could be right after the on-ramp or off-ramp. Descriptions of the highway segments are shown in Table 1.

Table 1. Raw observation data for the highway segments

Segment Order	Location	Type	Length km	Length miles	Raw Observed Data Volume (vph)			
1	I-235 EB at 50nd St NB	Starting point			4,500	5,000	5,500	6,000
2	Segment 1	Main	0.72	0.45	4,500	5,000	5,500	6,000
3	Exit 1B	Off-ramp			1,215	1,350	1,485	1,620
4	Segment 2	Main	0.75	0.47	3,285	3,650	4,015	4,380
5	I-235 EB at Valley West Dr SB	On-ramp			452	452	452	452
6	Segment 3	Main	0.33	0.21	3,737	4,102	4,467	4,832
8	I-235 EB at Valley West Dr NB	On-ramp			660	660	660	660
7	Segment 4	Main	0.50	0.31	4,397	4,762	5,127	5,492
9	Exit 2	Off-ramp			2,111	2,286	2,461	2,633
10	Segment 5	Main	0.99	0.62	2,286	2,476	2,666	2,859
11	I-235 EB at 22nd St	On-ramp			744	744	744	744
12	Segment 6	Main	0.66	0.41	3,030	3,220	3,410	3,603
13	Exit 3	Off-ramp			939	1,000	1,057	1,117
14	Segment 7	Main	0.55	0.34	2,091	2,222	2,353	2,486
15	I-235 EB at 8th St Loop	On-ramp			408	408	408	408
16	Segment 8	Main	0.38	0.24	2,499	2,603	2,761	2,894
17	Exit 4	Off-ramp			350	341	386	405
18	Segment 9	Main	1.07	0.66	2,149	2,262	2,375	2,489
19	I-235 EB at 63rd St	On-ramp			260	260	260	260
20	Segment 10	Main	1.47	0.91	2,409	2,522	2,635	2,749
21	I-235 EB at 42nd St	Off-ramp			554	580	606	632

Based on the method proposed by Shaw and Noyce (2014), the traffic volume of this study's corridor was balanced. The researchers provided the raw observation volume in Table 1 as well. Ramp length was not considered in the simulation scenarios and therefore is not shown in Table 1.

Vissim has two car-following models: Wiedemann 74 for urban traffic and Wiedemann 99 for freeway traffic. The Wiedemann 99 car-following model for freeway traffic was used in this study.

Driver behavior parameters were calibrated before simulation. The standstill distance (CC0), headway time (CC1), and following variation distance (CC2) parameters were found to have significant influences on traffic capacity in calibration. The calibrated CC0 was 3.05 meters (10.01 ft), CC1 was 1.45 seconds, and CC2 was 7.41 meters (24.31 ft). Additional details about the calibration can be found in Dong et al. (2015).

In the following simulation scenarios, real-time control to minimize fuel consumption was achieved by the following procedures. First, the traffic volume of each segment during time interval $[t_{n-1}, t_n]$ was collected by volume sensors installed before and after each entry or exit point where the vehicles were guided into or were leaving the main highway section. Second, desired vehicle density at t_n was obtained via Equation (38), which was assumed to be constant during $[t_n, t_{n+1}]$. Third, based on the current density information at t_n, CQOP formulated as Equation (36) was solved using quadratic programming so that optimized inflow and outflow could be determined. Fourth, desired density for t_{n+1} was calculated through Equation (38). In the last step, the desired speed during $[t_{n-1}, t_n]$ was obtained using Equation (39) and displayed $v_d(t_n, x_k)$ in the corresponding dynamic speed limit sign. The time interval to update the speed limit was 120 seconds.

To verify the improvement of fuel efficiency, the fuel consumption amount with and without the control strategy was recorded and compared. The default speed limit of the experimental section was 120 km/h (75 mph) for the case without speed control. For each scenario, the simulation was designed to last 4,200 seconds. Since traffic status was not stable at the beginning period, only the simulation results from 600 to 4,200 seconds were used for data analysis.

To demonstrate the feasibility of the proposed control strategy under heavy traffic volume, four scenarios corresponding to different volume demands were considered, which included original traffic on I-235 and vehicles entering from I-35N and 50th Street N (i.e., Scenario 1: 4,500 veh/h; Scenario 2: 5,000 veh/h; Scenario 3: 5,500 veh/h; and Scenario 4: 6,000 veh/h). Simulation results are discussed in the following section.

Simulation Results

As shown in Figure 4, a parallelogram region was determined by shifting the fitted speed-density line up and down. The speed could be slightly different from the theoretical result provided by linear regression in a neighboring region. Hence, to consider realistic application, optimal speed

values were rounded to the increment of 5 km/h (3 mph) and no less than 15 km/h (9 mph). Figures 6 through 9 demonstrate the density history with and without speed control for simulation Scenarios 1 through 4, respectively.
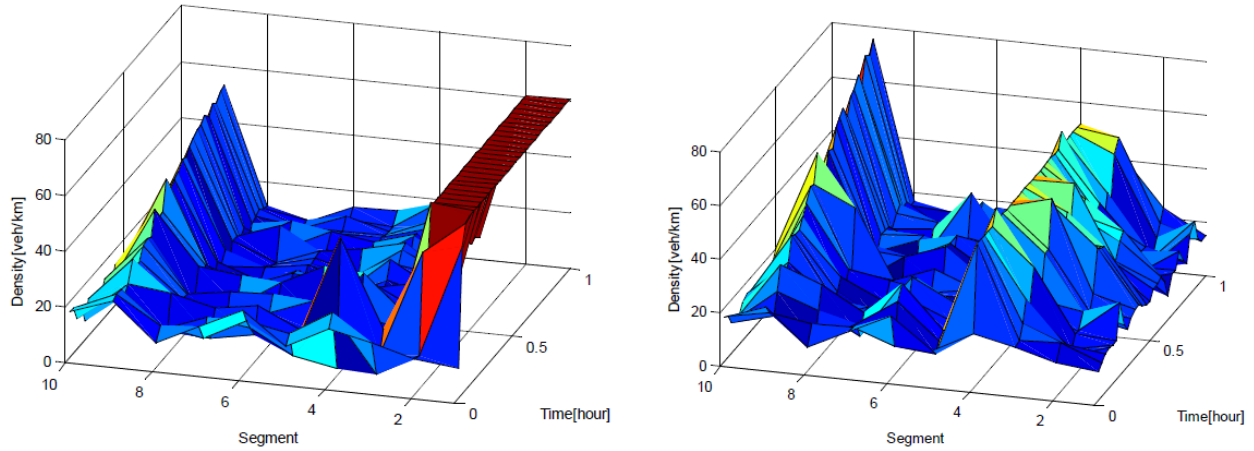

Figure 6. Density history of Scenario 1 with a starting volume of 4,500 veh/h: speed limit signs controlled by the rounded optimal solution (left) and an uncontrolled case with a desired speed of 120 km/h (75 mph) (right) for each segment
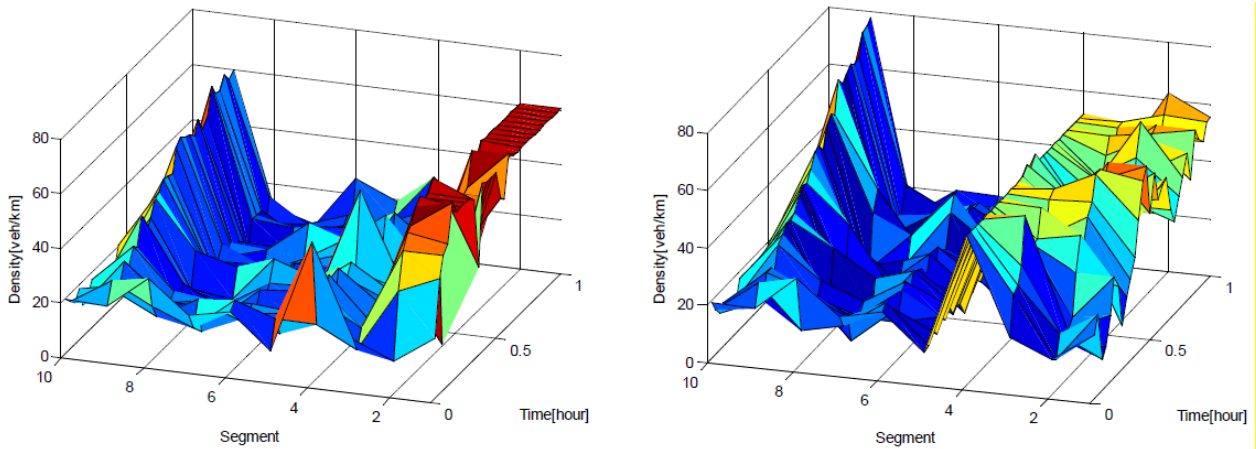
Figure 7. Density history of Scenario 2 with a starting volume of 5,000 veh/h: speed limit signs controlled by the rounded optimal solution (left) and an uncontrolled case with a desired speed of 120 km/h (75 mph) (right) for each segment

Figure 8. Density history of Scenario 3 with a starting volume of 5,500 veh/h: speed limit signs controlled by the rounded optimal solution (left) and an uncontrolled case with a desired speed of 120 km/h (75 mph) (right) for each segment

Figure 9. Density history of Scenario 4 with a starting volume of 6,000 veh/h: speed limit signs controlled by the rounded optimal solution (left) and an uncontrolled case with a desired speed of 120 km/h (75 mph) (right) for each segment
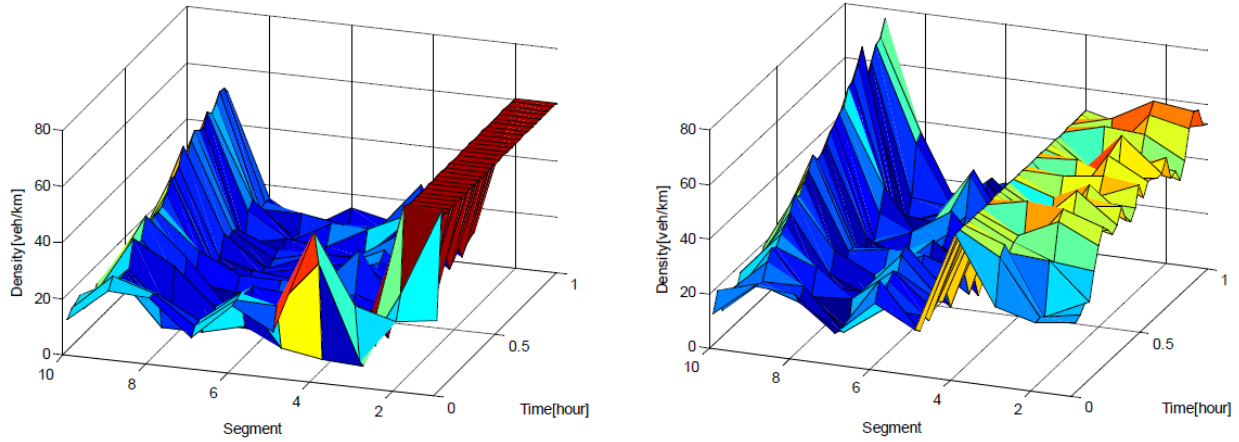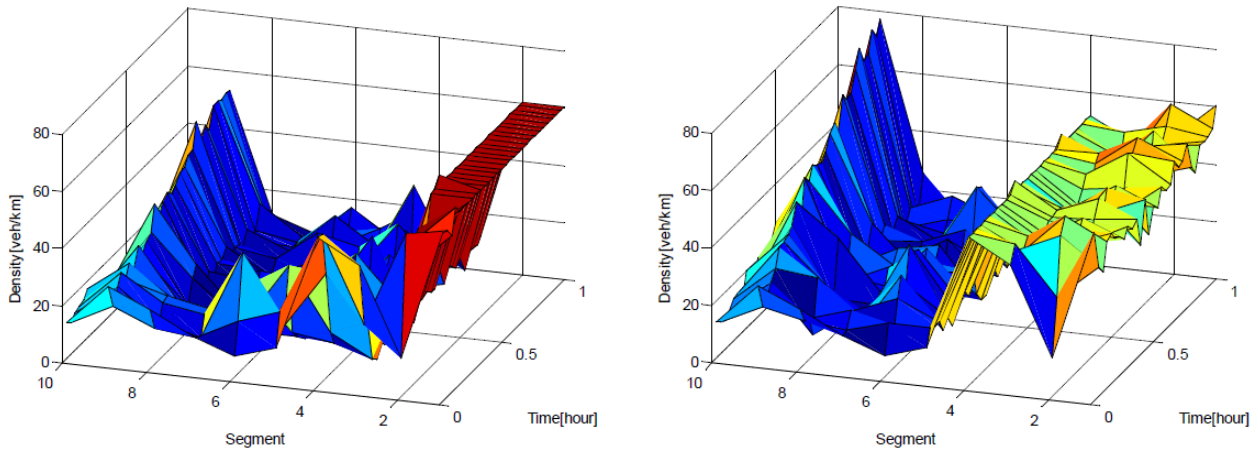
The density history diagram demonstrates the average density reduction along the experimental highway section. Compared to the uncontrolled strategy, the proposed control strategy led to lower average vehicle density, especially for Segment 9, which generated a high density value at the end of the simulation period. By implementing the proposed algorithm, severe congestion was avoided for that segment. Figures 7 through 9 demonstrate the improved performance of congestion alleviation in scenarios with relatively high demands ($\geq$ 5,000 veh/h).

The fuel consumption for all vehicles traveling along the experimental highway section during a one-hour interval is provided in Table 2.

Table 2. Total fuel consumption in simulation scenarios with and without control

Scenario	With Control (kg)	With Control (Gallons)	Without Control (kg)	Without Control (Gallons)	Reduction Percentage
	534.9	141.3	565.3	149.3	5.37%
	563.5	148.9	583.3	154.1	3.52%
Scenario 1:	557.0	147.1	564.4	149.1	1.32%
4,500 veh/h	556.5	147.0	571.9	151.1	2.69%
	564.9	149.2	594.1	156.9	5.17%
					Average: 3.61%
	579.2	153.0	622.6	164.5	6.97%
	543.9	143.7	625.7	165.3	13.06%
Scenario 2:	541.7	143.1	618.8	163.5	12.46%
5,000 veh/h	565.4	149.4	625.3	165.2	9.57%
	561.6	148.4	605.9	160.1	7.31%
					Average: 9.87%
	542.9	143.4	648.0	171.2	16.22%
	542.2	143.2	650.3	171.8	16.62%
Scenario 3:	552.8	146.0	640.3	169.1	13.66%
5,500 veh/h	557.1	147.2	649.3	171.5	14.20%
	553.1	146.1	645.1	170.4	14.26%
					Average: 14.99%
	553.5	146.2	652.9	172.4	15.22%
	547.1	144.5	648.0	171.2	15.57%
Scenario 4:	538.6	142.3	641.6	169.5	16.05%
6,000 veh/h	554.1	146.4	652.8	172.5	15.12%
	554.5	146.5	645.2	170.4	14.06%
					Average: 15.20%

In comparison to the case without control, the researchers' speed control strategy significantly reduced the fuel consumption amount on the highway segment. Meanwhile, the optimal solution could be obtained within an average of 1.8 seconds using MATLAB installed on a standard desktop computer with a 3.50 GHz processor and 16 GB RAM. The high computational performance indicated the capability for real-time implementation. Therefore, the proposed method was verified to be applicable to a range of large-scale, real-world traffic control scenarios.

The researchers selected five different seed parameters (without control and for the four different scenarios) to initialize five random number generators in Vissim. The different seed settings allowed them to simulate stochastic variations of vehicles entering the highway segment at the origin location. Five sets of comparison results are shown in Table 3 for Scenarios 1 through 4.

Table 3. T-test results in simulation scenarios with and without control

Scenario	(with control - without control) t-test	Reduction percentage t-test
Scenario 1: 4,500 veh/h	p-value = 0.0312 95% CI: (-38.50718, -2.37282)	
Scenario 2: 5,000 veh/h	p-value = 0.0002355 95% CI: (-80.60807, -41.99193)	Scenario 1 - 2: p-value = 0.005857 95% CI: (-0.11660199, -0.03054235)
Scenario 3: 5,500 veh/h	p-value = 4.612e-08 95% CI: (-105.33765, -88.62235)	Scenario 2 - 3: p-value = 0.009428 95% CI: (-0.10927944, -0.02296164)
Scenario 4: 6,000 veh/h	p-value = 1.89e-08 95% CI: (-107.36563, -89.71437)	Scenario 3 - 4: p-value = 0.7789 95% CI: (-0.02570897, 0.02016403)

CI = confidence interval

The researchers did a t-test for each scenario to statistically examine the performance of the proposed optimal control strategy. The p-value and 95% confidence interval (CI) are shown in Table 3. The t-test samples show fuel consumption amounts from five repeated simulations with the different seed parameters.

The t-test for the difference between the controlled and uncontrolled cases (second column in Table 3) showed that the p-value decreased when the demanding traffic volume increased. This decreasing trend demonstrates further fuel consumption reduction when compared to the uncontrolled case. Therefore, the proposed control strategy was more effective when applied in severely congested scenarios. Furthermore, the negative value of CI demonstrated the effectiveness of the proposed control strategy (i.e., fuel consumption is always reduced).

The t-test for reduction percentage (third column in Table 3) showed a significantly increasing p-value. The p-values of Scenarios 3 and 4 are greater than 0.05, which indicate the acceptance of the null hypothesis. Specifically, fuel consumption reduction converged to a stable state, which implies that no further reduction could have been achieved if the demanding volume continued to increase.

It was found that a lower reduction percentage value would likely be generated in Scenario 4 than in Scenario 3, according to the positive upper bound of the CI. However, a stable reduction percentage could have been achieved for scenarios with a demanding volume between Scenarios 3 and 4.

CONCLUSIONS

The researchers propose that an efficient distributed optimization method would minimize fuel consumption of the traffic flow modeled by the Lighthill-Whitham-Richard partial differential equation. This explicit solution to the Cauchy problem was based on the Lax-Hopf formula and Greenshields fundamental diagram. Linear model constraints to satisfy the initial and boundary conditions were considered in the Barron-Jensen/Frankowska solution.

After modeling the performance index as a quadratic function, the real-time, fuel-efficient traffic control problem was formulated as a convex quadratic optimization problem. The original CQOP (in a dual sense) was decomposed by introducing associated Lagrangian multipliers. Dual-decomposed subproblems were also formulated as CQOPs and could be iteratively solved through the subgradient method.

Simulation results demonstrated reduced fuel consumption and alleviated traffic congestion. The feasibility of the proposed optimization method was verified through the Vissim simulation tool, which considered different traffic volumes and random seed parameters.

Implementation Readiness

The proposed real-time highway control strategy can be implemented on highway sections using dynamic speed limit signs. The researchers plan to extend the one-dimensional control strategy to a highway network control strategy in the future.

The objective can be not only fuel consumption minimization, but also travel time minimization, throughput maximization, or multiple objectives. Moreover, the researchers expect to use hybrid highway infrastructures to design even more efficient control strategies, such as dynamic speed limit signs, ramp meters, and highway information signs.

REFERENCES

Alsabaan, M., K. Naik, and A. Nayak. 2010. Applying vehicular ad hoc networks for reduced vehicle fuel consumption. *Recent Trends in Wireless and Mobile Networks*, Vol. 84, pp. 217–228.

Barkenbus, J. N. 2010. Eco-driving: An overlooked climate change initiative. *Energy Policy*, Vol. 38, No. 2, pp. 762–769.

Barron, E. and R. Jensen. 1990. Semicontinuous viscosity solutions for Hamilton–Jacobi equations with convex Hamiltonians. *Communications in Partial Differential Equations*, Vol. 15, No. 12, pp. 293–309.

Barth, M., S. Mandava, K. Boriboonsomsin, and H. Xia, H. 2011. Dynamic ECO-driving for arterial corridors. *Proceedings of the IEEE Forum on Integrated and Sustainable Transportation System*, Vienna, Austria, June 29–July 1, pp. 182–188.

Bayen, A. M., C. Claudel, and P. Saint-Pierre. 2007. Computation of solutions to the Moskowitz Hamilton-Jacobi-Bellman equation under viability constraints. *Proceedings of the 46th IEEE Conference on Decision and Control*, December 12–14, New Orleans, LA, pp. 4737–4742.

Canepa, E. S. and C. G. Claudel. 2012. Exact solutions to traffic density estimation problems involving the Lighthill-Whitham-Richards traffic flow model using mixed integer programming. *Proceedings of the 15th International IEEE Conference on Intelligent Transportation Systems*, September 16–19, Anchorage, AK, pp. 832–839.

Claudel, C. G. 2010. *Convex formulations of inverse modeling problems on systems modeled by Hamilton-Jacobi equations: Applications to traffic flow engineering*. Ph.D. dissertation. University of California, Berkeley, CA.

Claudel, C. G. and A. M. Bayen. 2010a. Lax–Hopf based incorporation of internal boundary conditions into Hamilton–Jacobi equation. Part I: Theory. *IEEE Transactions on Automatic Control*, Vol. 55, No. 5, pp. 1142–1157.

Claudel, C. G. and A. M. Bayen. 2010b. Lax–Hopf based incorporation of internal boundary conditions into Hamilton-Jacobi equation. Part II: Computational methods. *IEEE Transactions on Automatic Control*, Vol. 55, No. 5, pp. 1158–1174.

Daganzo, C. F. 1994. The cell transmission model: A dynamic representation of highway traffic consistent with the hydrodynamic theory. *Transportation Research Part B: Methodological*, Vol. 28, No. 4, pp. 269–287.

Daganzo, C. F. 1995. Properties of link travel time functions under dynamic loads. *Transportation Research Part B: Methodological*, Vol. 29, No. 2, pp. 95–98.

Dai, R., J. Dong, and A. Sharma. 2015. Distributed traffic control for reduced fuel consumption and travel time in transportation networks. *Proceedings of the 2015 European Control Conference*, July 15–17, Linz, Austria, pp. 2658–2663.

Dong, J., A. J. Houchin, N. Shafieirad, C. Lu, N. R. Hawkins, and S. Knickerbocker. 2015. *Vissim Calibration for Urban Freeways*. Center for Transportation Research and Education, Institute for Transportation, Iowa State University, Ames, IA.

Greenshields, B. D., J. R. Bibbins, W. S. Channing, and H. H. Miller. 1935. A study of traffic capacity. *Proceedings of the 14th Annual Meeting of the Highway Research Board*, December 6–7, Washington, DC, Vol. 14, No. 1, pp. 448–477.

Guler, S. I., M. Menendez, and L. Meier. 2014. Using connected vehicle technology to improve the efficiency of intersections. *Transportation Research Part C: Emerging Technologies*, Vol. 46, pp. 121–131.

Li, C. and S. Shimamoto. 2012. An open traffic light control model for reducing vehicles' CO_2 emissions based on ETC vehicles. *IEEE Transactions on Vehicular Technology*, Vol. 61, No. 1, pp. 97–110.

Li, K., B. Chen, A. I. Sivakumar, and Y. Wu. 2014a. An inventory–routing problem with the objective of travel time minimization. *European Journal of Operational Research*, Vol. 236, No. 3, pp. 936–945.

Li, Y., E. Canepa, and C. Claudel. 2014b. Optimal control of scalar conservation laws using linear/quadratic programming: Application to transportation networks. *IEEE Transactions on Control of Network Systems*, Vol. 1, No. 1, pp. 28–39.

Lighthill, M. J. and G. B. Whitham. 1955. On kinematic waves. II. A theory of traffic flow on long crowded roads. *Proceedings of the Royal Society of London A: Mathematical, Physical and Engineering Sciences*, Vol. 229, No. 1178, pp. 317–345.

Lu, S-F., Q-P. Wei, W. Shen, and X-M. Liu. 2012. Integrated simulation platform of Vissim, Excel VBA, MATLAB. *Journal of Transportation Systems Engineering and Information Technology*, Vol. 12, No. 4, pp. 43–48.

Mazaré, P.-E., A. H. Dehwah, C. G. Claudel, and A. M. Bayen. 2011. Analytical and grid-free solutions to the Lighthill–Whitham–Richards traffic flow model. *Transportation Research Part B: Methodological*, Vol. 45, No. 10, pp. 1727–1748.

Ntziachristos, L., Z. Samaras, S. Eggleston, N. Gorissen, D. Hassel, and A. J. Hickman. 2000. COPERT III. *Computer Programme to calculate emissions from road transport, methodology and emission factors (version 2.1)*. Technical Report 49. European Environment Agency, Copenhagen, Denmark.

Ozatay, E., U. Ozguner, S. Onori, and G. Rizzoni. 2012. Analytical solution to the minimum fuel consumption optimization problem with the existence of a traffic light. *Proceedings of the ASME 2012 5th Annual Dynamic Systems and Control Conference with the JSME 2012 11th Motion and Vibration Conference*, October 17–19, Fort Lauderdale, FL, pp. 837–846.

Pasquale, C., S. Sacone, and S. Siri. 2014. Ramp metering control for two vehicle classes to reduce traffic emissions in freeway systems. *Proceedings of the 2014 European Control Conference*, June 24–27, Strasbourg, France, pp. 2588–2593.

Press, W., S. Teukolsky, W. Vetterling, and B. Flannery. 1992. *Numerical Recipes in Fortran 77: The Art of Scientific Computing*. Second Edition. Cambridge University Press, Cambridge, UK.

PTV AG. 2014. *PTV Vissim 7.0 User Manual*. PTV Group, Karlsruhe, Germany.

Richards, P. I. 1956. Shock waves on the highway. *Operations Research*, Vol. 4, No. 1, pp. 42–51.

Shaw, J. W. and D. A. Noyce. 2014. Automated optimal balancing of traffic volume data for large access-controlled highway networks and freeway-to-freeway interchanges. No. 14-3565. *Proceedings of the Transportation Research Board 93rd Annual Meeting*, January 12–16, Washington, DC.

Sims, A. G. and K. W. Dobinson. 1980. The Sydney coordinated adaptive traffic (scat) system philosophy and benefits. *IEEE Transactions on Vehicular Technology*, Vol. 29, No. 2, pp. 130–137.

Tettamanti, T. and I. Varga. 2012. Development of road traffic control by using integrated Vissim-MATLAB simulation environment. *Periodica Polytechnica Civil Engineering*, Vol. 56, No. 1, pp. 43–49.

Zegeye, S., B. De Schutter, J. Hellendoorn, E. Breunesse, and A. Hegyi. 2013. Integrated macroscopic traffic flow, emission, and fuel consumption model for control purposes. *Transportation Research Part C: Emerging Technologies*, Vol. 31, pp. 158–171.

Zegeye, S. K. 2011. Model-based traffic control for sustainable mobility. PhD dissertation. Delft University of Technology (TU Delft), Delft, Netherlands.

Zu, Y., R. Dai, and J. Dong. 2016a. Convex optimization for energy-efficient traffic control. *Proceedings of the 55th IEEE Conference on Decision and Control*, December 12–14 Las Vegas, NV.

Zu, Y., C. Liu, A. Sharma, R. Dai, and J. Dong. 2016b. Real-time energy-efficient traffic control via convex optimization. *IEEE Transactions on Intelligent Transportation Systems*, Under Review

THE INSTITUTE FOR TRANSPORTATION IS THE FOCAL POINT FOR TRANSPORTATION AT IOWA STATE UNIVERSITY.

InTrans centers and programs perform transportation research and provide technology transfer services for government agencies and private companies;

InTrans manages its own education program for transportation students and provides K-12 resources; and

InTrans conducts local, regional, and national transportation services and continuing education programs.

INSTITUTE FOR TRANSPORTATION

IOWA STATE UNIVERSITY

Visit **www.InTrans.iastate.edu** for color pdfs of this and other research reports.